RP Current Trends In Applied Sciences (e-ISSN: 2583-7486)
Vol. 5, No. 1 (January – March 2026) pp. 18–25

RESEARCH PLATEAU PUBLISHERS

Cite this article: Ramon González Calvet, Adsorption isotherm deduced from the billiard model and its generalization to real gases, *RP Cur. Tr. Appl. Sci.* **5** (2026) 18–25.

Original Research Article

Adsorption isotherm deduced from the billiard model and its generalization to real gases

Ramon González Calvet

Institut Pere Calders, Campus Universitat Autònoma de Barcelona, 08193 Cerdanyola del Vallès, Spain
*Corresponding author, E-mail: rgonzalezcalvet@gmail.com

ARTICLE HISTORY
Received: 16 March 2026
Revised: 27 May 2026
Accepted: 27 May 2026
Published: 12 June 2026

KEYWORDS
Billiard isotherm; Adsorption; Hard-sphere gas; Lennard-Jones potential; Virial coefficients; Soft-sphere gas.

ABSTRACT
Billiard balls moving freely on a table are a model for simulating the adsorption of spherical molecules on a surface. Simulations provide the free-area function (the ratio of the area available for the center of an additional molecule to the total area) as function of coverage. The billiard adsorption isotherm differs from the Langmuir isotherm in that it takes into account the translational entropy instead of the configurational entropy. Its generalization to three dimensions is the gas of hard spheres. The dependence of the free-volume function on density is not linear as assumed by Van der Waals, but a higher-degree polynomial. However, molecules in real gases are soft and behave like elastic balls. The Lennard-Jones potential allows us to model the attractive forces and how the free volume increases with temperature. From here, a reduced equation of state is obtained that is universal for all gases.

1. Introduction

Several adsorption isotherms have been proposed to describe the adsorption of compounds and ions on surfaces. In order to describe the adsorption of some gases (nitrogen, methane, carbon monoxide, argon, oxygen, and carbon dioxide) on glass at 90K and on mica at 155K, Langmuir [1] proposed in 1918 the isotherm $\theta/(1-\theta)=\beta a$ assuming that N molecules adsorb at M fixed sites on the surface ($N \le M$). Here, $\theta = N/M$ is the *coverage*, a is the bulk phase activity (usually approximated by concentration), and β is the *adsorption coefficient* only depending on the nature of the compound, the nature of the surface and the temperature. The configurational entropy of the adsorption layer is then obtained from the number of combinations, $S = k \ln C_M^N$ [2, p. 127]. In 1925, Frumkin [3] added to the Langmuir isotherm an interaction term similar to the attractive term a/V^2 in the Van der Waals equation of real gases

$$\frac{\theta}{1-\theta}\exp(-B\theta)=\beta a \qquad (1)$$

Frumkin already showed that, for $B > 4$, his adsorption isotherm predicts a phase transition between a very dilute phase and a phase with coverage close to unity. Since then, many other isotherms have been proposed, of which 14 were listed by Damaskin et al. [4, pp. 86-88]. In the case of ionic adsorption, the virial isotherm $\ln\Gamma + B\Gamma = \ln\beta + \ln a$ has been widely used because it does not have as parameter the maximum surface excess Γ_{max}, which is usually unknown and has a lot of uncertainty in the case of ions. The *surface excess* is $\Gamma = N/(N_0 A)$ where A is the area of the surface and N_0 is the Avogrado number. With a modified Frumkin isotherm with two factors related to the interfacial electric field that we will not explain here owing to lack of space, we were able [5] to reproduce well the adsorption of chloride and iodide on the mercury electrode and their capacity curves but with strange values of the maximum surfaces excess. For chloride we used a maximum adsorption charge of $\sigma_1^{max} = -0.40\ \mathrm{C.m^{-2}}$ and $B = 0$ while the charge of a hexagonal compact lattice of chloride ions deduced from the ionic radius is $\sigma_1^{comp} = -1.4118\ \mathrm{C.m^{-2}}$. For iodide we used $\sigma_1^{max} = -0.40\ \mathrm{C.m^{-2}}$ and $B = -7.16$, while the charge of a hexagonal compact lattice of iodide ions is $\sigma_1^{comp} = -0.9556\ \mathrm{C.m^{-2}}$. This paradox remained unsolved for many years until a game of billiards played with a friend revealed the solution.

2. Simulations of the Billiard Model

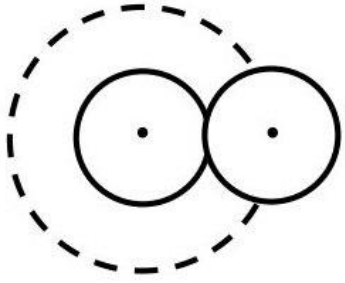

Figure 1: The centers of two spheres cannot be closer than their diameter.

Halide ions are spherical with closed electronic shells. Their adsorption was first studied from aqueous solutions on the dropping mercury electrode [6]. Mercury is a liquid metal with a homogeneous unstructured surface that must be considered plane. On the other hand, the halide adsorption studies were carried out at room temperature [7, 8, 9], much higher than the temperature ranges studied by Langmuir. His hypothesis of localized adsorption is not realistic for halide ions on mercury, which we expect to be delocalized. Therefore, billiard balls on a table seem to be a good model for them. We assumed that halide ions are hard spheres with radii equal to their ionic radii that only interact by contact (like the collision of billiard balls) and electrostatically (since they are charged). They can move freely on the surface and have translational energy like billiard balls rolling on the table, reaching any point unless it is already occupied by another ball. When the surface is empty, the total area A is available to the first ball. If one ball is already present on the surface, the area available to the center of the second ball is $A-4\pi R^2$ (R is the radius of the balls) because it cannot approach the first center at a distance less than $2R$ (Figure 1). If there are N balls on the surface, the available *free area* is approximately $A_{\text{free}} \cong A-4\pi NR^2$ if $4\pi NR^2 << A$. That is, the exclusion area of each ball is four times its projection onto the surface, and the maximum surface excess appears to be much smaller than that corresponding to the hexagonal compact packing. This is the puzzling phenomenon observed in the adsorption of chloride and iodide.

We define the *coverage* as a molar fraction equal to the ratio of the number of balls on the surface to the maximum number in the compact lattice. The area of the rhombic cell containing one ball in a compact hexagonal lattice is $A_{\text{cell}} = 2\sqrt{3}R^2 \cong 3.4641R^2$, larger than the area πR^2 of the ball's projection onto the surface due to interstitial spaces. Therefore, the coverage is $\theta = \Gamma / \Gamma_{\text{comp}} = A_{\text{cell}} N / A = 2\sqrt{3}\, N R^2 / A$. We also define the *shadow* φ [10] as the ratio of the shaded area to the total area when a zenithal light illuminates the billiard table, that is, $\varphi = \pi N R^2 / A$. Shadow is proportional to coverage since $\varphi = \pi\theta/(2\sqrt{3})$. While $0 \le \theta \le 1$, shadow does not reach unity because $0 \le \varphi \le \pi/(2\sqrt{3}) = 0.9069$ owing to the interstitial holes between spheres.

We define the *free-area function* as the quotient of the area available to the center of a new ball to be added to the surface divided by the total area. At low coverage, it is

$$f(\theta) = \frac{A_{\text{free}}}{A} \cong 1 - \frac{4\pi NR^2}{A} = 1 - \frac{2\pi}{\sqrt{3}}\theta = 1 - 4\varphi$$

$$\text{if} \quad \theta << 1 \qquad (2)$$

When coverage increases, intersections between exclusion circles having radius $2R$ of different spheres are more frequent and the free-area function separates from this linear law. There is no easy way to calculate the free-area function so that we resorted to simulations.

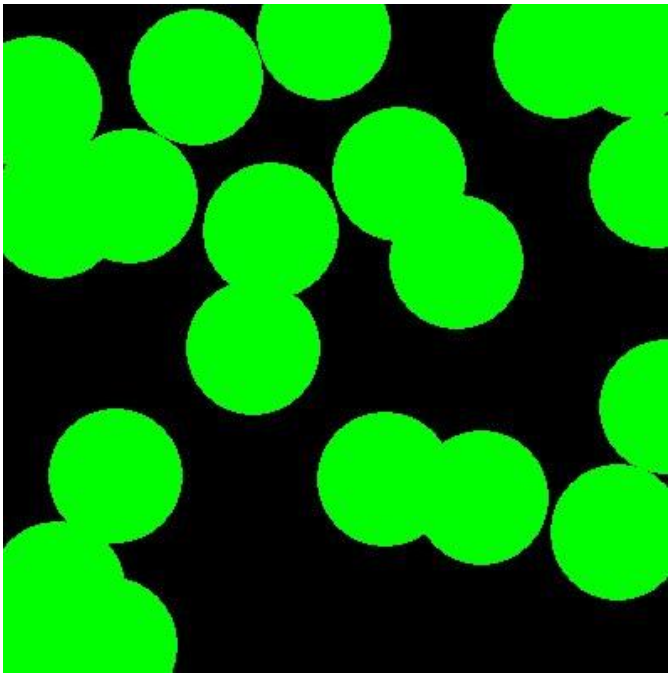

Figure 2: Halfway through the simulation. The exclusion circles with radius $2R = 0.1$ in green and the free area in black.

Simulations of a random distribution of billiard balls on a table were carried out by painting exclusion circles of radius $2R$ on a square of unity side on the computer screen (Figure 2) and checking that all the distances between their centers are greater than $2R$. The pixels of the square are scanned each time a new exclusion circle is added until exhausting the free area. Since periodic boundary conditions can generate periodic patterns, we chose random boundary conditions: Exclusion circles were painted with centers in the square $[0,1]^2$, but the scanned pixels only belong to the square $[2R, 1-2R]^2$. The frame of width $2R$ [11] helps to set up random boundary conditions but is not useful for pixel counting (in [12] we took an insufficient width R). The free area function is the ratio of unpainted pixels to scanned pixels. The chosen radius was $R = 0.05$ and the scanning grid size was 0.005. Other values of R only mean widening or shortening the scale at which we look at the surface but do not change the results. The variability in the values of the free-area function is reduced by running many simulations. The function obtained from the average of 100 simulations is shown in Figure 3. On average, the free area is exhausted at $\theta_{\max} \cong 0.57$, although this value depends on each simulation. More details of simulations can be found in [11, 12].

3. Statistical Thermodynamics and Adsorption Isotherm

The translational partition function of a particle i adsorbed on a surface having an area A_i is $z_i = A_i / \Lambda^2$ where $\Lambda = h/\sqrt{2\pi\, mkT}$ is the thermal wavelength, h is the Planck constant, m is the mass of the particle, k is the Boltzmann constant and T is the absolute temperature.

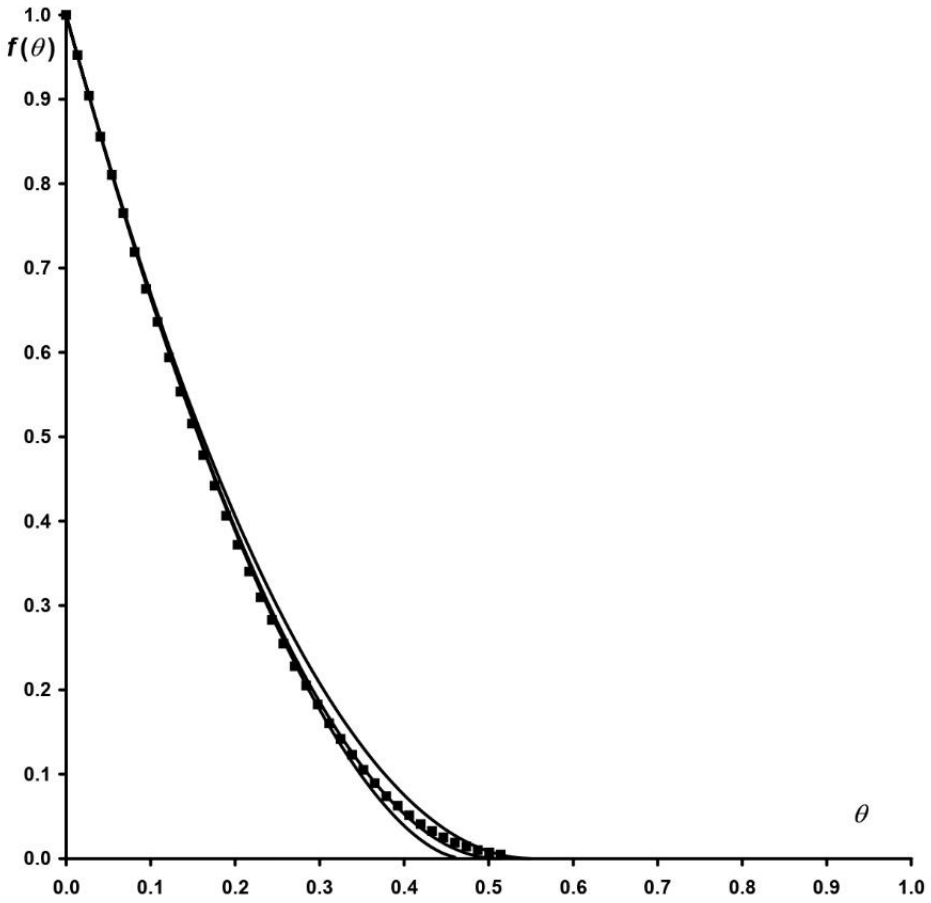

Figure 3: Free-area function versus coverage obtained by averaging 100 simulations (squares) compared with the quadratic (upper line), the cubic (middle line), and the power-law (lower line) approximations.

The total area A is available to the first particle added to the surface, but the free area available to a new particle progressively decreases as more particles are adsorbed. The free area available to the particle i is $A_i = A\,f(\theta_i)$, where $\theta_i = iA_{\text{cell}}/A = 2i\sqrt{3}R^2/A$. The translational partition function of a system of N independent particles having different available areas A_i is

$$Z_N = \frac{\prod_{i=1}^{N} z_i}{N!} = \frac{A^N}{N!\Lambda^{2N}} \prod_{i=1}^{N} f(\theta_i) \tag{3}$$

and already includes Gibbs' correction for indistinguishable particles. The Helmholtz energy is the logarithm of the partition function of the system

$$F = -kT \ln Z_N = kT\left(N \ln \frac{\Lambda^2}{A} + N \ln N - N - \sum_{i=1}^{N} \ln f(\theta_i) \right) \tag{4}$$

Approximating the sum by an integral gives

$$F = NkT\left(\ln \frac{\Lambda^2}{A_{cell}} + \ln\theta - 1 \right) - \frac{kTA}{A_{cell}} \int_0^{\theta} \ln f(\theta_i)\, d\theta_i \tag{5}$$

where $\theta = NA_{cell}/A$. Since $dF = -S\,dT - p\,dA + \mu\,dN$, the chemical potential of the adsorption layer is

$$\mu = \left(\frac{\partial F}{\partial N} \right)_{T,A} = kT\left(\ln \frac{\Lambda^2}{A_{\text{cell}}} + \ln\theta - \ln f(\theta) \right) \tag{6}$$

which is equal to that of the solution $\mu = \mu_0 + kT \ln a$ yielding the adsorption isotherm

$$\frac{\theta}{f(\theta)} = \beta a \quad \text{with} \qquad \beta = \frac{A_{\text{cell}}}{\Lambda^2} \exp\frac{\mu_0}{kT} \tag{7}$$

Similarly, the surface pressure $p = \gamma_0 - \gamma$ (the difference between the surface tension in the absence and presence of adsorption) is obtained as

$$p = -\left(\frac{\partial F}{\partial A} \right)_{N,T} = \frac{NkT}{A}\left(1 - \frac{1}{\theta} \int_0^{\theta} \frac{\theta_i\, f'(\theta_i)}{f(\theta_i)}\, d\theta_i \right) \tag{8}$$

and the compressibility factor of this two-dimensional gas of hard spheres is

$$\frac{pA}{NkT} = 1 - \frac{1}{\theta} \int_0^{\theta} \frac{\theta_i\, f'(\theta_i)}{f(\theta_i)}\, d\theta_i = 1 - \frac{1}{\varphi} \int_0^{\varphi} \frac{\varphi_i\, f'(\varphi_i)}{f(\varphi_i)}\, d\varphi_i \tag{9}$$

The virial coefficients $B_{2,\rho}$ are the coefficients of the expansion $p/kT = \rho + B_{2,\rho}\rho^2 + B_{3,\rho}\rho^3 + \cdots$ in terms of the number density $\rho = N/A$. The virial coefficients $B_{n,\rho}$ have

dimensions of $(m^3)^{n-1}$. For a hard-sphere gas, the dimensionless virial coefficients of the expansion

$$\frac{pA}{NkT} = 1 + B_2\varphi + B_3\varphi^2 + \cdots \tag{10}$$

in terms of the shadow $\varphi = \pi R^2 \rho$ are $B_n = B_{n,\rho} / \left(\pi R^2\right)^{n-1}$. Over the past century, several of them were calculated in different works. A summary of these results given as the quotients $B_{n,\rho} / B_{2,\rho}^{n-1}$ can be found in [13]. Since $B_{2,\rho} = 2\pi R^2$ and $B_2 = 2$ (corresponding to the linear law $f(\varphi) \cong 1 - 4\varphi$ at low coverage), the dimensionless virial coefficients are then obtained from these quotients by means of $B_n = 2^{n-1} B_{n,\rho} / B_{2,\rho}^{n-1}$. Identifying (9) with (10) allows us to find the free-area function from the virial coefficients

$$f(\varphi) = \exp\left(-\sum_{n=2}^{+\infty} \frac{n}{n-1} B_n \varphi^{n-1} \right). \tag{11}$$

4. Polynomial Approximations to the Free-Area Function

The free-area function averaged from simulations fits a quadratic function with high correlation but it depends on each set of simulations. The quadratic function tangent to the abscissa axis[1] that tends to the linear law (2) at low coverage is unique

$$f(\theta) = \left(1 - \frac{\pi}{\sqrt{3}}\theta\right)^2 = (1 - 2\varphi)^2 = 1 - 4\varphi + 4\varphi^2 \tag{12}$$

and goes to zero at $\theta_{\max} = \sqrt{3}/\pi \cong 0.5513$ or $\varphi_{\max} = 0.5$. A better approximation is a cubic. The expansion of the exponential of the virial series with $B_2 = 2$, and $B_3 = 16/3 - 4\sqrt{3}/\pi$ up to second order is

$$f(\varphi) = \exp\left(-2B_2\varphi - \frac{3B_3}{2}\varphi^2 - \cdots \right) = 1 - 4\varphi + \frac{6\sqrt{3}}{\pi}\varphi^2 + \cdots \tag{13}$$

The second-degree coefficient is now lower than 4. Every realistic approximation to $f(\varphi)$ must satisfy $f(\varphi_{\max}) = f'(\varphi_{\max}) = 0$, which determines the cubic coefficient

$$\begin{aligned} f(\varphi) &\cong 1 - 4\varphi + \frac{6\sqrt{3}}{\pi}\varphi^2 + 1.439544\varphi^3 \\ &= 1 - \frac{2\pi}{\sqrt{3}}\theta + \frac{\pi\sqrt{3}}{2}\theta^2 + 1.0737480\theta^3 \end{aligned} \tag{14}$$

with $\varphi_{\max} \cong 0.464039$ or $\theta_{\max} \cong 0.511676$. This cubic fits the simulation data better but predicts a lower maximum coverage than determined from simulations ($\theta_{\max} \cong 0.57$). Figure 3 compares the free-area function obtained from simulations with the quadratic and cubic approximations. At medium coverages, the quadratic approximation slightly overestimates the free-area function obtained from simulations but for practical purposes, it is quite accurate and much better than $f(\theta) = 1 - \theta$ predicted by the Langmuir isotherm.

Another possible approximation is a power law. Identifying the first two coefficients of the expansion in terms of φ, one finds a power law with a smaller exponent than for the quadratic law

$$f(\varphi) = \left(1 - \frac{4\varphi}{t}\right)^t = \left(1 - \frac{2\pi}{\sqrt{3t}}\theta\right)^t \quad \text{with} \quad t = \frac{4\pi}{4\pi - 3\sqrt{3}} = 1.705020\ldots \tag{15}$$

which predicts $\varphi_{\max} \cong 0.426255$ and $\theta_{\max} \cong 0.470013$ and is far from what is obtained from simulations.

5. The Free-Volume Function of a Hard-Sphere Gas

When a spherical particle is added to an empty volume, it can move freely throughout the volume. When a second particle is added to the volume, the two centers cannot come closer than $\sigma = 2R$, so the exclusion sphere of the first particle has eight times its volume. Therefore, the free-volume function for a dilute hard-sphere gas is

$$f(\eta) \cong 1 - \frac{32\pi NR^3}{3} = 1 - 8\eta \quad \text{for} \quad \eta << 1 \tag{16}$$

where $\eta = 4\pi NR^3/3 = N\pi\sigma^3/6$ is called the *packing fraction*, which is similar to the shadow φ. A close packing of hard spheres can form a hexagonal lattice or a face-centered cubic lattice, which have the same density. The volume of the rhombohedral cell containing one sphere of radius R in these lattices is $V_{\text{cell}} = 4\sqrt{2}R^3 \cong 5.6568R^3$, which is larger than the volume of the sphere $4\pi R^3/3 \cong 4.1888R^3$ due to the interstitial spaces. We define the *filling* as the ratio of the number of spheres in a given volume to their number in a compact lattice, that is, $\psi = NV_{\text{cell}}/V = 4\sqrt{2}NR^3/V$. The filling is a molar fraction that generalizes the coverage to three dimensions, and satisfies $0 \le \psi \le 1$. The filling and the packing fraction are proportional according to $\eta = \pi\psi/(3\sqrt{2})$. The packing fraction satisfies $0 \le \eta \le \pi/(3\sqrt{2}) \cong 0.7405$.

The free-volume function is the probability that any point is available to the center of a new sphere, and this probability can be approximated by the relative frequency of available points in any subset of the three-dimensional space. Thus, three different kinds of simulations were carried out to determine the free-volume function by scanning a cube, a square or a segment. Scanning a cube is slow and exclusion spheres cannot be painted on the computer screen, while pixels can be scanned in the other two cases. Scanning a segment is fast, but the results are highly variable. A description of all three programs can be found in [11]. The optimal program consists of locating

[1]Since coverages greater than 0.57 are not impossible, but only improbable and do sometimes occur, the free-area function should approach the abscissa axis asymptotically like (13) or, at least, should be tangent to it. Therefore, it cannot intersect the abscissa axis.

centers of hard spheres in the box[2] $[0,1]^2\times[-2\sigma, 2\sigma]$ shown in Figure 4, always ensuring that every additional center is not closer than $\sigma = 2R$ to all other centers previously placed in the box. If (x, y, z) are the validated random coordinates of the center of a new sphere, then the circle of radius $\sqrt{\sigma^2 - z^2}$ and center (x, y) that is the intersection of the exclusion sphere with the plane $z = 0$ is painted on the computer screen (Figure 5). Then, scanning the pixels of the square $[\sigma, 1-\sigma]^2$ yields the free-volume function. The thermodynamic deduction of the equation of state of a hard-sphere gas in a volume is the same as for two dimensions but with $z_i = V_i / \Lambda^3$. Therefore

$$f(\eta) = \exp\left(-\sum_{n=2}^{+\infty} \frac{n}{n-1} B_n \eta^{n-1}\right) \tag{17}$$

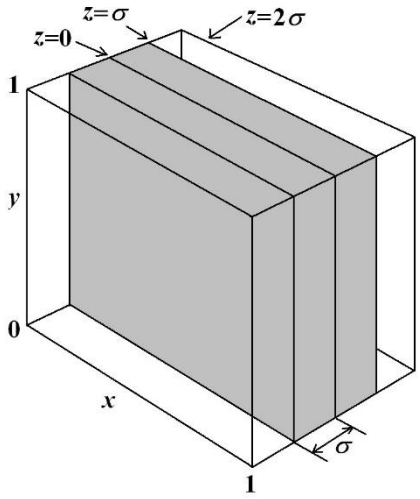

Figure 4: Simulation box containing the centers of exclusion spheres. Only those whose centers lie in the grey box cut the plane $z = 0$.

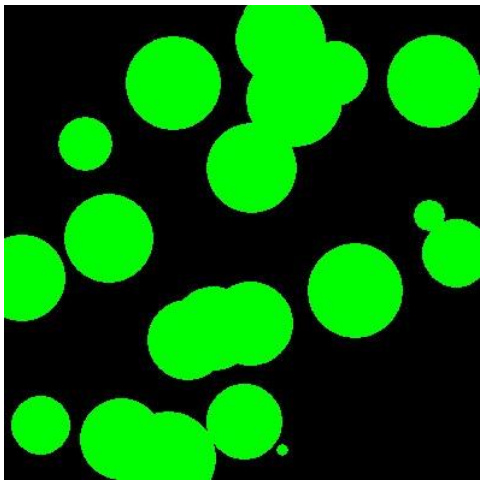

Figure 5: Central plane $z = 0$ of the box in Fig. 4. Exclusion spheres of radius $\sigma = 0.1$ intersect this plane in the green circles.

Tian et al. gave the virial coefficients up to B_{12} [14] with high accuracy except for the last one. Boltzmann [15, p. 352] already calculated $B_2 = 4$ and $B_3 = 10$, and Van Laar calculated the corresponding free-volume function [16, Equation 11]

$$\frac{pV}{NkT} = 1 + 4\eta + 10\eta^2 + \cdots \quad \Leftrightarrow$$
$$f(\eta) = 1 - 8\eta + 17\eta^2 + \cdots \tag{18}$$

The agreement between the free-volume function obtained from simulations and from the virial coefficients is excellent as shown in Figure 6.

Van der Waals assumed that the free volume available to n moles of gas is the linear law $V - nb$, where b is a constant called *covolume*. However, the free-volume function is not linear except at low densities. A power law gives the best fitting with an exponent 8/3, that is, $f(\eta) = (1-3\eta)^{8/3}$ and the resulting equation of state is

$$\frac{pV}{NkT} = -\frac{5}{3} - \frac{8}{9\eta}\ln(1-3\eta) \tag{19}$$

Hard spheres do not take into account either the attractive intermolecular forces or the variation of the exclusion sphere with temperature. To take them into account, a model of the intermolecular interaction is needed.

6. Gas of Soft Spheres

Molecules behave like hard spheres at low temperatures and like elastic balls at higher temperatures. Instead of billiard balls, a more appropriate model would be tennis balls. For spherical molecules, the interaction energy depends only on the distance r between their centers. To describe the intermolecular interaction we have chosen the Lennard-Jones potential $u(r) = 4\varepsilon[(\sigma/r)^{12} - (\sigma/r)^6]$, where σ is the distance at which the potential is zero, and ε is the depth of the potential well. The second virial coefficient for any radial intermolecular potential is [2, Equation 15-24 on p. 267]

$$B_{2,\rho} = -\frac{1}{2}\int_0^{+\infty}\left(\exp\left(-\frac{u(r)}{kT}\right) - 1\right) 4\pi r^2 dr \tag{20}$$

Vargas et al. [7] calculated an exact expression of the second virial coefficient as function of the modified Bessel functions. However, our approximation explained below is easier to be implemented. First at all, we split the integration interval into two intervals. For $r < \sigma$ the potential $u(r)$ is repulsive and divergent, while for $r > \sigma$ the potential is attractive and remains bounded, $-\varepsilon/kT \le u(r) \le 0$, so that they require different analytic approximations. In the repulsive interval, integration by parts gives

$$\begin{aligned} B_{2,\rho}^r &= -\frac{1}{2}\int_0^{\sigma}\left(\exp\left(-\frac{u(r)}{kT}\right) - 1\right) 4\pi r^2 dr \\ &= \frac{1}{2}\int_0^{+\infty} \frac{4\pi\left[r(u)\right]^3}{3}\exp\left(-\frac{u}{kT}\right)\frac{du}{kT} \end{aligned} \tag{21}$$

[2]First, we took the box $[0,1]^2\times[-\sigma, \sigma]$ [11], but later we realized that the random boundary conditions require a larger box, which we corrected in [10].

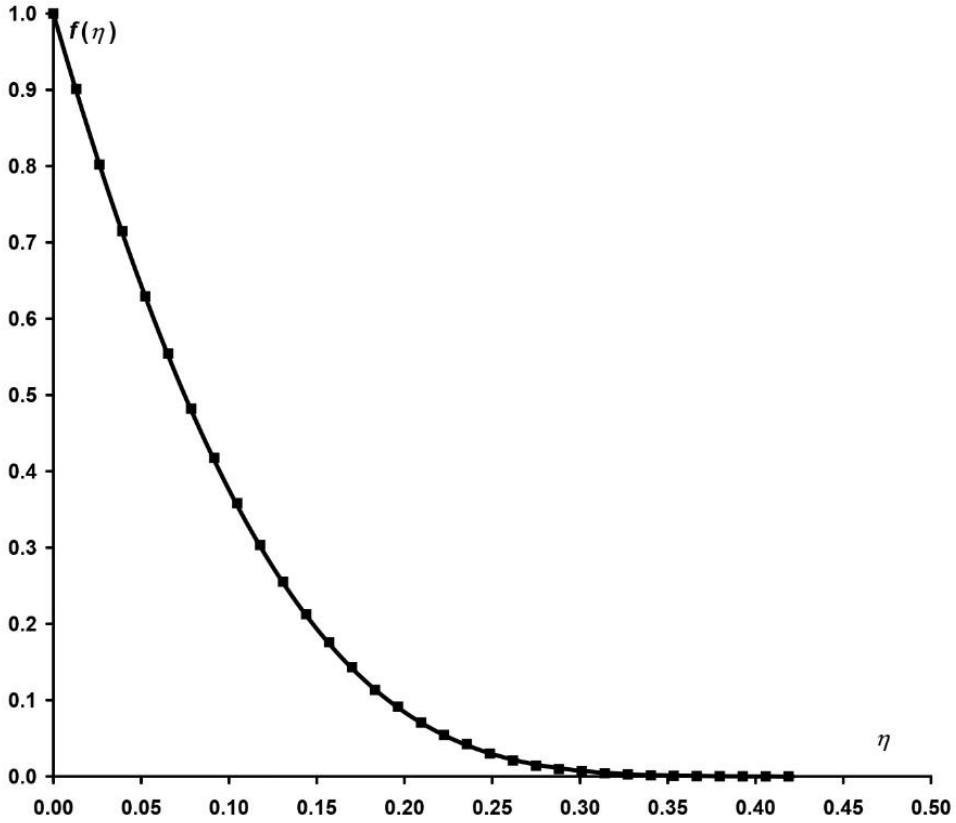

Figure 6: Free-volume function versus packing fraction. Squares obtained by averaging 100 simulations. Line calculated from the exponential (17) of virial coefficients.

where $r(u)$ is the inverse function of $u(r)$. For the Lennard-Jones potential, it is

$$r(u)=\frac{\sigma}{\sqrt[6]{\frac{1+\sqrt{1+u/\varepsilon}}{2}}} \tag{22}$$

If we interpret $\exp(-u/kT)/kT$ like a probability density [8, p. 128], then the repulsive part of the second virial coefficient is equal to half the volume of the exclusion sphere averaged for all positive energies.

$$B_{2,\rho}^{r}=\frac{1}{2}\left\langle\frac{4\pi r^3}{3}\right\rangle=\frac{2\pi\sigma^3}{3g(\tau)} \qquad \text{with}$$

$$g(\tau)\cong\sqrt{\frac{1+\sqrt{1+0.5\ln(1+\tau)+0.5\tau}}{2}} \tag{23}$$

By means of numerical integration, we have found a better approximation to $g(\tau)$ than in [11], where $\tau=kT/\varepsilon$ is the dimensionless temperature. The higher the relative energy u of two particles, the smaller the minimum distance their centers can reach just like two tennis balls. In this sense, the Lennard-Jones potential provides a model for the elasticity of molecules. For the attractive part of the second virial coefficient, the expansion of the exponential gives the approximation [11]

$$\begin{aligned}B_{2,\rho}^{a}&=-\frac{1}{2}\int_{\sigma}^{+\infty}\left(\exp\left(-\frac{u(r)}{kT}\right)-1\right)4\pi r^2dr\\&\cong-\frac{16\pi\sigma^3}{9\tau}-\frac{128\pi\sigma^3}{315\tau^2}-\frac{1024\pi\sigma^3}{10395\tau^3}.\end{aligned} \tag{24}$$

The dimensionless coefficient is $B_2^a=6B_{2,\rho}^a/(\pi\sigma^3)$. By adding this approximation of B_2^a and introducing $\eta=\pi<r^3>\rho/6=\eta_0/g(\tau)$ into (19), we have found an equation of state of real gases [10] that satisfies the principle of the corresponding states and reproduces qualitatively the curves of the compressibility factor (Figure 7)

$$\begin{aligned}\frac{pV}{NkT}&=-\frac{5}{3}-\frac{8g(\tau)}{9\eta_0}\ln\left(1-\frac{3\eta_0}{g(\tau)}\right)\\&\quad-\left(\frac{32}{3\tau}+\frac{256}{105\tau^2}+\frac{2048}{3465\tau^3}\right)\eta_0.\end{aligned} \tag{25}$$

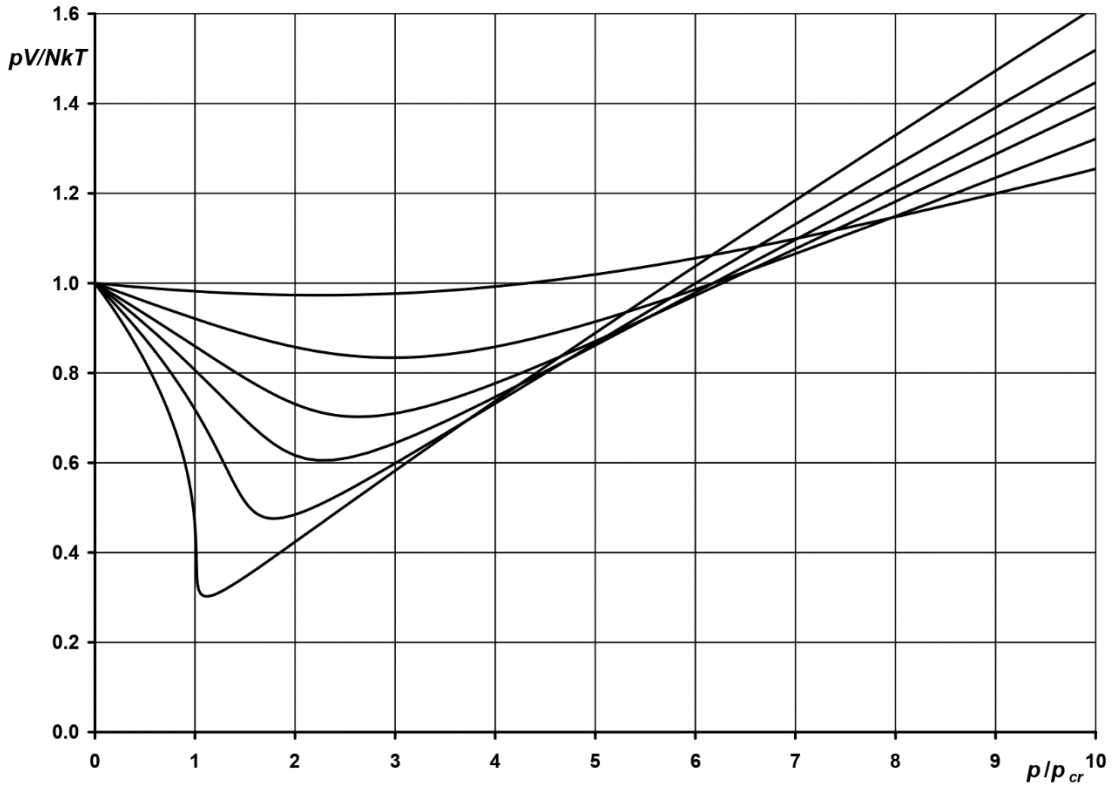

Figure 7: Compressibility factor versus reduced pressure calculated from (25) for reduced temperatures T/T_{cr} equal to 1, 1.1, 1.2, 1.3, 1.5 and 2.

However, the calculated minima are higher and the crossing of the different curves takes place at lower pressures than in experimental data [19, Fig. 1.6 on p. 26], [20, Fig. 3.1 on p. 45]. Our compressibility factor calculated at the critical point is 0.3710 lower than 0.375 for the van der Waals equation, while the experimental values are slightly lower than 0.3 for many gases. This result is expected since only the second virial coefficient is taken into account to describe the attraction between molecules, which is insufficient. In conclusion, an equation of state of a hard-sphere gas improved with the variation of the exclusion radius with temperature (soft spheres) and with the attractive part of the second virial coefficient already gives a good qualitative description of real gases, although the agreement is not yet quantitative.

Authors' contributions

The author read and approved the final manuscript.

Conflicts of interest

The author declares no conflict of interest.

Funding

This research received no external funding.

Data availability

No new data were created.

References

[1] I. Langmuir, The adsorption of gases on plane surfaces of glass, mica and platinum, *J. Am. Chem. Soc*. **40** (1918) 1361–1403.
[2] T.L. Hill, *An Introduction to Statistical Thermodynamics*, Dover, New York (1986).
[3] A.N. Frumkin, Die Kapillarkurve der höheren Fettsäuren und die Zustandsgleichung der Oberflächenshicht, *Z. Phys. Chem*. **116** (1925) 466–484.
[4] B.B. Damaskin, O.A. Petrii, V.V. Batrakov, *Adsorption of Organic Compounds on Electrodes*, Plenum Press, New York (1971).
[5] F. Sanz, R. González, Theoretical considerations of the adsorption isotherm for ionic systems at electrode interphases, *Electrochim. Acta* **34** (1989) 1883–1887.
[6] D.C. Grahame, Die elektrische Doppelshicht, *Z. Elektrochem*. **59** (1955) 773–778.
[7] R. Payne, Specific adsorption of chloride ions at the mercury/aqueous solution interface, *Trans. Faraday Soc*. **64** (1968) 1638–1655.
[8] A.R. Sears, Ph.A. Lyons, The adsorption of potassium bromide from constant ionic strength solutions of potassium bromide and potassium fluoride, *J. Electroanal. Chem*. **42** (1973) 69–76.
[9] E. Dutkiewicz, R. Parsons, The adsorption of iodide ion from aqueous KI + KF of constant ionic strength, *J. Electroanal. Chem*. **11** (1966) 100–110.
[10] R. González Calvet, El billar como modelo para la adsorción de moléculas esféricas y su generalización a los gases reales, *Contrib. Cienc. Soc*. **19** (2026) 1–22.
[11] R. González, Ecuaciones de estado de un gas bidimensional y tridimensional de esferas rígidas, in: *Perspectivas e Inovação na Pesquisa em Química*, Atena Editora (2025) pp. 53–76.
[12] R. González, Adsorption isotherm deduced from the billiard model, *Electrochim. Acta* **524** (2025) 145917.
[13] E.J. Janse van Rensburg, Virial coefficients for hard disks and hard spheres, *J. Phys. A* **26** (1993) 4805–4818.
[14] J. Tian, H. Jiang, M. Mulero, Equations of state of hard sphere fluids based on recent accurate virial coefficients B_5–B_{12}, *Phys. Chem. Chem. Phys*. **21** (2019) 13070–13077.
[15] L. Boltzmann, *Lectures on Gas Theory*, Dover, Mineola (1995).
[16] L. Boltzmann, On the characteristic equation of van der Waals, *Proc. Koninklijke Nederlandse Akademie van Wetenschappen* **1** (1898) 398–404.

[17] P. Vargas, E. Muñoz, L. Rodríguez, Second virial coefficient for the Lennard–Jones potential, *Physica A* **290** (2001) 92–100.
[18] A.M. Vasilyev, *An Introduction to Statistical Physics*, URSS, Moscow (1994).
[19] D. Kondepudi, *Introduction to Modern Thermodynamics*, Wiley, Chichester (2008).
[20] G.M. Kontogeorgis, G.F. Folas, *Thermodynamic Models for Industrial Applications*, Wiley, Chichester (2020).